Optical Wireless Channel Simulation for Communications inside Aircraft Cockpits

Pierre Combeau, Steve Joumessi-Demeffo, Anne Julien-Vergonjanne, Lilian Aveneau, Stéphanie Sahuguède, Hervé Boeglen and Damien Sauveron

***Abstract*—Communications inside an aircraft cockpit are currently based on wired connections especially for the audio headsets used by the pilots. A wireless headset would be an advantage in terms of comfort and flexibility but the use of classical radio frequencies is limited by interference and security issues. Optical wireless communication technology is an option for headset connectivity. Indeed, as optical beams are confined, this technology provides robustness against the risk of hacking, thus increasing security. In addition, the use of optical waves ensures the absence of radio-frequency disturbances. Using simulation, this paper presents a thorough study of the optical wireless channel behavior inside the cockpit of an aircraft by considering a headset worn by a pilot possibly in motion and an access point at the ceiling. The impact of the characteristics of the environment model, such as the level of geometric description, the reflectivity of materials and for the first time, the ambient noise induced by the sun, is highlighted. System performance is evaluated in terms of optimal half-power angles and the necessary average optical power of the light sources.**

***Index Terms*—Optical wireless communication, Infrared transmissions, Channel modelling, Simulation.**

I. Introduction

TODAY, it is accepted that the exponential development of wireless communications could lead to saturation of the radio-frequency (RF) spectrum currently available [1]. Among the solutions under consideration for future wireless networks, the use of an unregulated optical spectrum, covering the ultraviolet (UV), infrared (IR) and visible bands is a heavily studied option [2]. Optical wireless communications (OWCs) are suitable for a wide range of use cases, offering unique functionality, especially in indoor environments. Indeed, in hospital, industrial or aeronautical scenarios, OWCs obviously offer a robustness to electromagnetic interference and to hacking of communications, because of the confinement of optical waves [3]–[6].

Several projects have focused on the deployment of OWCs in aircraft. These projects have generally focused on cabin communications as in-flight connectivity can offer new services to passengers [7]–[12].For example, the studied scenarios included entertainment applications [7], video broadcasting [8], communication between passengers [9], and even medical surveillance [10]. One of the main challenges in the context of an aircraft is to ensure adequate coverage of the cabin environment, which requires a thorough analysis of the communication channel [11]. Many factors affect the quality of the optical channel, such as the geometry of the environment, the reflectance properties of the materials, and the parameters of the sources and receivers. The environment can also be dynamic, causing changes to these parameters that can affect the channel. These considerations become very important for a new use case in an aircraft that involves pilots in the cockpit.

Currently, connections in the cockpit are essentially wired, especially with regard to audio communications with and between pilots. A wireless headset would bring comfort and mobility to the pilots, which is important on long-haul flights. The crew's effectiveness would be improved especially in critical phases such as take-off or landing. OWC technology has advantages in this scenario because there is no interference with or disruption of existing radio-frequency connections. In addition, it is robust against hacking problems and can therefore offer a higher level of security than RF signals used for Bluetooth headset for example. Actually, a major drawback of RF signals is their sensitivity to attacks from the physical layer such as listening and jamming because RF waves can penetrate through walls, thus exposing the information conveyed by these signals to hackers [13]. One way to improve the security against eavesdropping is at the physical layer, where optical technology has advantages because, unlike RF systems, optical signals are blocked by opaque objects and therefore cannot pass through walls. Safety against external eavesdropping can therefore be improved if no light escapes from the cockpit.

For critical flight phases such as take-off and landing, the brightness is reduced to accommodate pilots' eyes in the dark, in the event of an electrical failure. Thus, to communicate in this context, the visible band is not appropriate; the IR one is preferable.

In [14], and for the first time in the literature, a study of the 940 nm optical channel for wireless communications inside an aircraft cockpit was presented. This simulation study showed the feasibility of bidirectional audio communication between the devices included in the pilots headsets and an access point (AP) on the cockpit ceiling, using spatial diversity on the headset side. Based on the simulated channel gains, the optimal characteristics of the sources, in terms of half-power angles were determined. Then, using an on-off keying (OOK) modulation with a fixed transmission power, the maximum achievable data rate was evaluated according to the desired

Manuscript received September 13, 2019; revised April 5, 2020; revised May 25, 2020; accepted June 14, 2020. This work was funded by the European Union under Grant 737645, through the Cleansky2 H2020 project titled Aircraft Light Communication (ALC).

P. Combeau, L. Aveneau and H. Boeglen are with the XLIM laboratory, UMR CNRS 7252, University of Poitiers, France e-mail: (pierre.combeau@univ-poitiers.fr)

S. Joumessi-Demeffo, A. Julien-Vergonjanne, S. Sahuguède and D. Sauveron are with the XLIM laboratory, UMR CNRS 7252, University of Limoges, France.

quality of service (QoS).

However, this former study has some shortcomings in its approach to the propagation channel modeling:

- The results presented in [14] were obtained for a 3D full detailed environment model, corresponding to a huge amount of data, often private and so not accessible, which leads to heavy computational effort;
- All the materials were considered as perfectly diffuse surfaces with a single reflectivity value of 0.5;
- A single dynamic scenario (pilot's head movement) was studied, with no true mobility inside the cockpit;
- The level of ambient optical noise was fixed, according to the literature, to the measured value in a conventional indoor environment at ground level, which differs from the proposed application;
- The analyses were based on analytical cumulative density functions (CDF) of channel gain, fitted to simulated data. Consequently, the minimum values of the CDFs used for the worst case, were under-estimated, which may have led to biased conclusions about the need for spatial diversity.

In this article, instead of considering spatial diversity, we deepen and extend the analysis of the optical wireless channel. The objective is to study the impact of the characteristics of the propagation environment on the specifications and performance of the connected headset system. The first characteristic of interest is the level of detail of the geometric description of the propagation environment model. In addition to the full detailed cockpit model, we consider a more schematic one of equivalent volume and shape, and assess their relative impacts. The second characteristic of interest concerns the reflective properties of the cockpit materials, which are usually poorly known, especially for such complex environments. Surfaces are considered to be perfectly diffuse with variable reflectivities, but also dielectric in terms of the windscreen, which is made of glass. Then, a new dynamic scenario relating to the pilot's body movements in his seat, and a full mobility scenario inside the cockpit are proposed and investigated. Next, the sun's contribution to the ambient optical noise level inside the cockpit is evaluated by simulation, for the first time in the literature. Finally, all the analyses are based on real simulated link budgets, unlike those conducted in [14].

The paper is organized as follows. The description of the communication system, along with the channel modelling and the analysis principle for channel behavior, are presented in Section II. Section III focuses on the determination of the optimal half-power angles of the sources depending on the propagation environment model and the reflective properties of the cockpit's materials. Section IV details the overall performance analysis of the system in a generic manner, independent of the considered modulation. The approach is based on a signal-to-noise ratio (SNR) evaluation, with specific attention to the ambient noise due to solar radiation. Then, using a specific level of QoS, it assesses the necessary optical emission power, still with regard to the propagation environment model but also taking into account the reflective properties of the cockpit's materials. Power is a critical specification of the system in terms of autonomy and eye safety. Lastly, Section V concludes this paper.

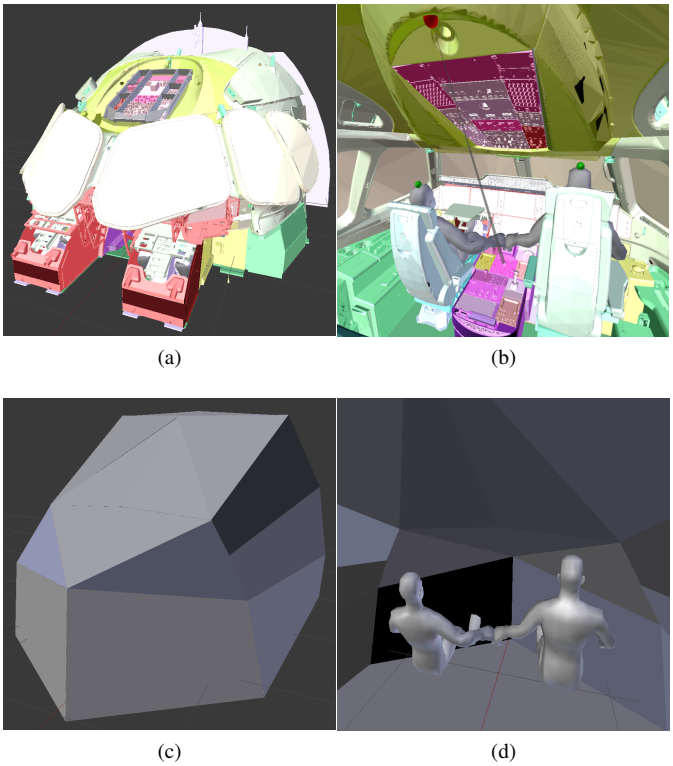

Fig. 1. (a) Outside 3D view of AIRBUS A350 cockpit, (b) inside 3D view including flight crew, with transceivers on the top of the pilots' headsets (green spheres) and on the ceiling (red sphere), (c) outside 3D view of the simplified cockpit, (d) inside 3D view including crew members.

II. Optical channel analysis

A. System description

The studied environment is a modern AIRBUS[1] A350 cockpit as illustrated in Fig.1(a). In this context, we focus on a scenario using optical wireless links to ensure the connectivity of headsets worn by the aircraft crew (see Fig.1(b)). We suppose that at least one member of the crew wears a headset continuously during flights. Therefore, it is important to assess link robustness.

In the following, we consider bidirectional IR links at 940 nm between the transceiver (T_x/R_x) integrated on the headset and the AP located on the cockpit ceiling. To avoid interferences between downlink and uplink, the chosen protocol is based on time sharing in a half-duplex master-slave network where the master is the AP and the slaves are the headsets. The method for the AP consists of a regular succession of downlink transmissions to each headset one after the other, followed by their responses in uplink. The most efficient IR configuration is when the emitted optical beam is directly in the field of view (FOV) of the receiver, corresponding to a line-of-sight (LOS) link. However, when using directed sources, LOS links require careful alignment of transceivers, resulting in a small coverage and high sensitivity to blockages. Because of headset mobility linked to pilot movements, the

[1]European aircraft manufacturer

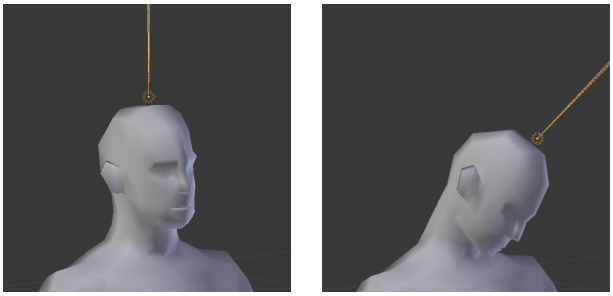

(a) (b)

Fig. 2. (a) Transceiver configuration at the headset, (b) random orientation due to pilot movements.

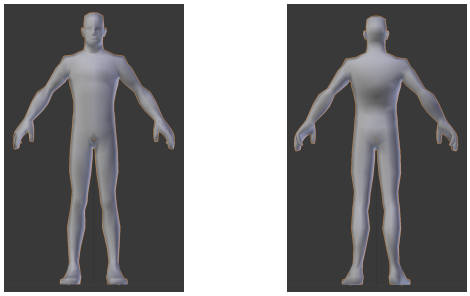

Fig. 3. 3D body model (1004 polygons).

LOS condition cannot always be fulfilled. Therefore, non line-of-sight (NLOS) links have to be considered. Thus, in the specific cockpit environment, multipath contributions are taken into account, according to the distance between the transceivers, their respective characteristics and orientations, LOS and multi-reflected (NLOS) contributions on cockpit elements, and the presence and movements of the pilot and co-pilot.

We first investigate an uplink between transmitters located on the top of the headsets and a receiver, located on the AP at about 1 m from the top of the pilots and co-pilots heads. It can be seen in Fig.1(b) that the pilot and co-pilot seats have very different settings, which represent the two limits of seat configurations. The pilot is the furthest from the control panel (his/her face is at 60 cm) at the lowest height (the top of the head is 40 cm below the ceiling and 1.17 m above the floor). The co-pilot is the closest to the control panel (his/her face is at 45 cm) and at the greatest height (the top of the head is 15 cm below the ceiling, and 1.30 m above the floor).

We also examine the downlink for the same positions, the receiver being either on the pilot's or the co-pilot's headset.

For both links, the orientations of transmitters and receivers at the AP are identical and fixed (black dotted line in Fig.1(b)). In contrast, the transmitter and the receiver on the headset are oriented perpendicular to the top of the pilot's head (see Fig.2(a)); therefore their orientation may vary randomly depending of the pilot's movements (see Fig.2(b)).

Whatever the link, the pilot and co-pilot are considered as potential sources of blockages because of their movements.

B. Channel modelling

To determine the channel impulse response, we adopt a modeling approach based on a stochastic Monte-Carlo method, associated with the ray-tracing algorithm. Our research laboratory has developed the RaPSor software (Ray Propagation Simulator), which is an extensible tool based on the Netbeans platform and coded in Java, for modelling wave propagation in realistic environments in different frequency domains, from the radio range to the optical one, in IR and in visible wavelengths [15]–[19]. This software allows determination of the impulse response $h(t)$ for a defined link.

The following inputs are required for the simulation: geometric model and reflection characteristics of the simulation environment, including pilot and co-pilot, definitions of key features as the maximum number of successive reflections, and the characteristics/locations of the optical transceivers.

1) Geometric models: The detailed 3D geometric model of the cockpit (see Fig.1(a) and (b)) is first generated from a STEP file, a classical CAO data format provided by AIRBUS in the context of the Aircraft Light Communication research project [20] funded by the European Union. It is then imported into RaPSor.

This model represents a very large amount of data: 3.3 million polygons stored in a 283 MB file. Its disadvantages are mainly related to the fact that these data are private and sensitive, and therefore often inaccessible to researchers outside of contractual frameworks. In addition, and as indicated in Section I, it is interesting to determine whether such a model is necessary for the implementation of the OWC system inside the cockpit. As a result, a second, much simpler geometric model is considered as illustrated in Fig.1(c) and (d). It is composed of only 20 polygons, and generally represents the shape of the cockpit, according to its main dimensions, without considering the furniture and onboard equipment.

In addition to the cockpit itself, important parameters affecting optical propagation are the pilots' bodies and the changes in transceiver orientation resulting from the pilots' movements. The body model representing the pilot and co-pilot is a 3D realistic human mesh of 1.8 m height and composed of 1004 polygons (see Fig.3). It was fully articulated and animated using the Blender software [21] in order to take into account realistic dynamic scenarios in our channel simulations. The choice of human body height doesn't really matter. As mentioned in Section II-A, the pilot and co-pilot seats are in extreme configurations. This applies particularly to the co-pilot's, which corresponds to a worst case scenario because his head is so close to the ceiling (15 cm) that the optical contributions arrive with a grazing incidence on the headset receiver. Regardless of the co-pilot's size, the headset transceivers cannot be closer to the ceiling. In contrast, the pilot's seat is at the lowest and most distant height from the control panel. In this configuration, the transceivers can more easily collect the different optical contributions. In conclusion, the behavior of the channel for a pilot of given size is located between the two studied configurations which can be considered as limits.

2) Reflection properties of materials: The windscreen is modelled in pure glass with a refractive index of 1.5, thus

as a dielectric material reflecting the incident light in a single direction according to the Snell-Descartes laws. To characterize the rays' reflection on the windscreen, we use the Fresnel coefficients [22], given by:

$$r_s = \frac{n_1 \cos\theta_i - n_2 \cos\theta_t}{n_1 \cos\theta_i + n_2 \cos\theta_t}, r_p = \frac{n_1 \cos\theta_t - n_2 \cos\theta_i}{n_1 \cos\theta_t + n_2 \cos\theta_i}, \quad (1)$$

where r_s and r_p are the reflection coefficients for s- and p-polarized light, n_1 and n_2 are the refractive indices of the incident and refracting media, and θ_i and θ_t are the incident and refracting angles. Considering un-polarized light, the overall reflection coefficient applied to the incident luminance is:

$$R_{diel} = \frac{1}{2}(|r_s|^2 + |r_p|^2). \quad (2)$$

All other surfaces in the scene are considered as perfectly diffuse. They are consequently modeled by a Lambertian bidirectional reflectance distribution function (BRDF) [18]. In a first approach and as in [14], we fixed the reflectivity values of the cockpit surfaces and the human bodies at 0.5, which is an average between perfectly absorbent and perfectly reflecting materials [19]. A specific study of the reflectivity value's impact is presented in Sections III and IV.

3) Optical sources and receivers properties: The optical characteristics of the transceivers are: their radiation pattern, particularly their semi-angle at half-power $\theta_{\frac{1}{2}}$; and the surface area of the photodetector.

In this study, we consider generalized Lambertian optical sources. The radiant intensity (W.sr^{-1}) from the transmitter T_x in a solid angle ω is given by [23]:

$$R_0(\omega) = P_t G_{T_x}(\omega), \quad (3)$$

with P_t the total optical emitted power in W, and G_{T_x} the radiation pattern of the source, depending of the azimuth and elevation angles ϕ and θ, with regard to the emitter's orientation:

$$G_{T_x}(\omega) = G_{T_x}(\phi, \theta) = \frac{(m+1)}{2\pi} \cos(\theta)^m. \quad (4)$$

The value of m is linked to $\theta_{\frac{1}{2}}$ by:

$$m = \frac{-\log(2)}{\log(\cos(\theta_{\frac{1}{2}}))}. \quad (5)$$

The receiver is a generic IR photodiode whose physical detection area is 7 mm^2. Its FOV defined at the half power semi-angle is 60°.

4) Dynamic scenarios: For a given half-power angle $\theta_{\frac{1}{2}}$, we can obtain from the simulations a set of impulse responses $h(t)$ corresponding to different IR links according to the orientation changes of the headset transceivers induced by the pilots' movements and by crew mobility inside the cockpit. Three scenarios are considered.

The first one, called "Head movement", is illustrated in Fig.4. It represents the set of potential positions/orientations of the pilot/co-pilot's head during the flight: pilot/co-pilot first looks ahead and then turns his/her head to the left, then tilts it forward, and then turns it to the right before returning it to its initial position.

Fig. 4. Illustration of pilot/co-pilots head movement.

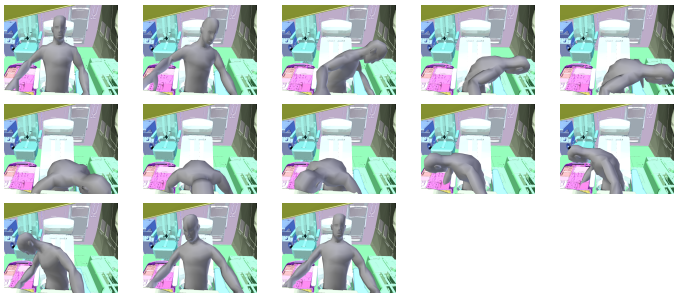

Fig. 5. Illustration of pilot/co-pilots body movement.

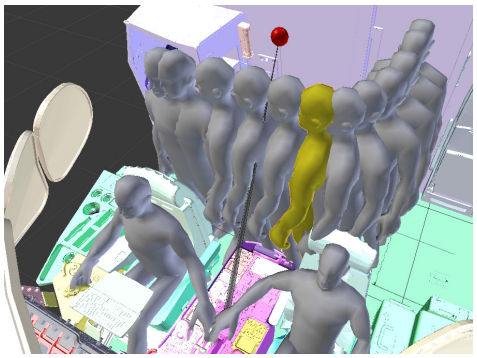

Fig. 6. Illustration of mobility inside the cockpit. The yellow represented position of the moving crew member fully obstructs the direct AP-Pilot link.

The second scenario, called "Body movement", is illustrated in Fig.5. Its objective is not to represent positions/orientations with high occurrence, but rather the extreme ones that may nevertheless occur during a flight, but not during critical phases; for instance when the pilot/co-pilot has to lean to the ground to pick up a fallen object.

The third scenario, illustrated in Fig.6, is a full mobility scenario corresponding to a person walking inside the cockpit while the two pilots are fixed in straight position; for example, another crew member. In this case the moving body may behave as a major obstacle to the LOS link. Among the blocking positions, the one that most obstructs the pilot-AP link is shown in yellow in Fig.6.

5) Considered number of reflections: For all the simulations, we consider a maximum number of 3 successive reflections, which is a classical approach when considering NLOS transmissions and has been found to be sufficient for simulation convergence [24].

C. Channel behavior analysis

One of the main parameters characterizing the optical channel is the gain, which determines the achievable SNR for a fixed transmitter power [25]. It is defined as:

$$H(0) = \int_{-\infty}^{+\infty} h(t)dt = H_0, \tag{6}$$

where $h(t)$ represents the channel impulse response, and $H(f)$ the channel frequency response.

Other features are time dispersion parameter related to impulse response length and mean delay spreading. The temporal dispersion induced by the reflected paths can be ignored for the cockpit use-case (audio communications) because of the relatively low signal bandwidth. We thus only focus on the channel gain.

The set of impulse responses $h(t)$ resulting from movements of the pilots leads to a set of optical gains H_0. Therefore, H_0 is statistically analyzed and the channel behavior is characterized using the statistical distribution.

In this work, we analyze the IR link reliability based on the optical gain cumulative density function CDF(H_0) defined as:

$$\text{CDF}(H_0) = \int_{-\infty}^{H_0} p(h_0)dh_0, \tag{7}$$

where $p(h_0)$ is the probability density function of H_0. CDF(H_0) represents the probability that the channel gain is lower than a given value H_0. The system reliability is increased at the highest possible gain values with the highest probability. Consequently, the smaller the CDF(H_0) for a given H_0, the higher the reliability. In the context of this article, the wireless headset system aims for 100% reliability in critical phases such as take-off and landing, meaning that communication must be ensured for the worst channel case as a function of pilot movements; i.e., for the minimum channel gain corresponding to CDF(H_0) $= 0$. As mentioned in Section I, this value is under-estimated when we consider the theoretical statistical laws as in [14]. For this reason, only the simulated gains are taken into account in this study to calculate the CDFs.

III. Study of optimal half-power angle

In this section, we investigate the IR channel behavior according to the two environment models of Fig.1 detailed in Section II-B1. This investigation concerns an uplink between a single emitter (T_x) on the top of the headset and a single receiver (R_x) at the AP, and a downlink between T_x at the AP and R_x on the top of the headset. In both configuration, the analysis is performed with respect to the half-power angle $\theta_{\frac{1}{2}}$ of the emitter T_x, the R_x's one being fixed to 60°. This analysis is applied to the three scenarios (head/body movements and full mobility) presented in Section II-B4, according to the characteristics of the environment.

A. Full detailed model

1) Scenario 1, head movement: Fig.7(a) and (b) show the channel gain CDF for the pilot, for the uplink and the downlink respectively. For the uplink, the transmitter orientations randomly vary according with head movements, whereas the receiver orientation is fixed (since the receiver remains fixed on the cockpit ceiling). The inverse applies for the downlink.

With regard to the uplink, Fig.7(a) shows that the channel gain CDF is degraded as the half-power angle of the emitter on the headset reduces. As an example, considering a gain value of -60 dB, the CDF value is higher than 75% for $\theta_{\frac{1}{2}} \leq 30°$. The CDF is reduced to 59% for $\theta_{\frac{1}{2}} = 60°$ which is the optimal angle in this configuration (as indicated above, the objective of 100% reliability requires choosing the half-power angle corresponding to the highest H_0 gain for CDF(H_0) =0).

For the downlink, Fig.7(b) shows similar behavior to the uplink, but with a smaller gap between curves for $\theta_{\frac{1}{2}} > 10°$. For example, although the channel gain value corresponding to the smaller CDF is obtained for the optimal angle $\theta_{\frac{1}{2}}$ equal to 40°, the second best $\theta_{\frac{1}{2}}$ being 50° have a gain difference of only 0.04 dB.

Fig.7(c) and 7(d) illustrate the channel gain CDF obtained for the co-pilot position, for the uplink and the downlink respectively. For the co-pilot position, the channel gain is degraded compared to the pilot's, especially for the uplink. As an example, for the uplink configuration, Fig.7(c) shows that for a gain value of -60 dB, the lowest CDF value for the co-pilot is 73% whereas it is 59% for the pilot. However, the optimal half-power angle obtained for the co-pilot is the same as that for the pilot for the uplink, i.e. $\theta_{\frac{1}{2}} = 60°$.

Fig.7(d) illustrates that for the downlink, channel performance is quite similar to the uplink, with the same weak gap between the curves when $\theta_{\frac{1}{2}} > 10°$, as it was already noted for the pilot. Indeed, the two best $\theta_{\frac{1}{2}}$ of 30° and 40° present a gain difference of only 0.09 dB. Thus, to have a common system in downlink for both pilot and co-pilot, we consider an overall optimal angle $\theta_{\frac{1}{2}}$ of 40°.

2) Scenario 2, body movement: Fig.8(a) and 8(b) show the channel gain CDFs for the uplink and downlink for the pilot, respectively, according to the second scenario in Fig.5, representing body movements.

As for the head movement scenario, the optimal $\theta_{\frac{1}{2}}$ appears to be respectively 60° for the uplink and 40° for the downlink. Also, although the overall behavior is the same, the channel performance is significantly less than with scenario 1 (head movement). Indeed, whereas scenario 1 produced 59% of gain values H_0 below -60 dB according to the pilot/uplink, scenario 2 gives 86% (see Fig.7(a) and 8(a)). Similarly, with the downlink, 55% of gain values H_0 were below -60 dB for the scenario 1, while they were about 83% for the scenario 2 (see Fig.7(b) and 8(b)).

Similar observations can be seen in the co-pilot results provided in Fig.7(c) and (d) and Fig.8(c) and (d).

3) Scenario 3, full mobility: Beyond the movements that pilots can perform in their seats during the flight, it is important to evaluate the potential impact of full body mobility inside the cockpit, illustrated in Fig.6.

This article has been accepted for publication in a future issue of this journal, but has not been fully edited. Content may change prior to final publication. Citation information: DOI 10.1109/JLT.2020.3003989, Journal of Lightwave Technology

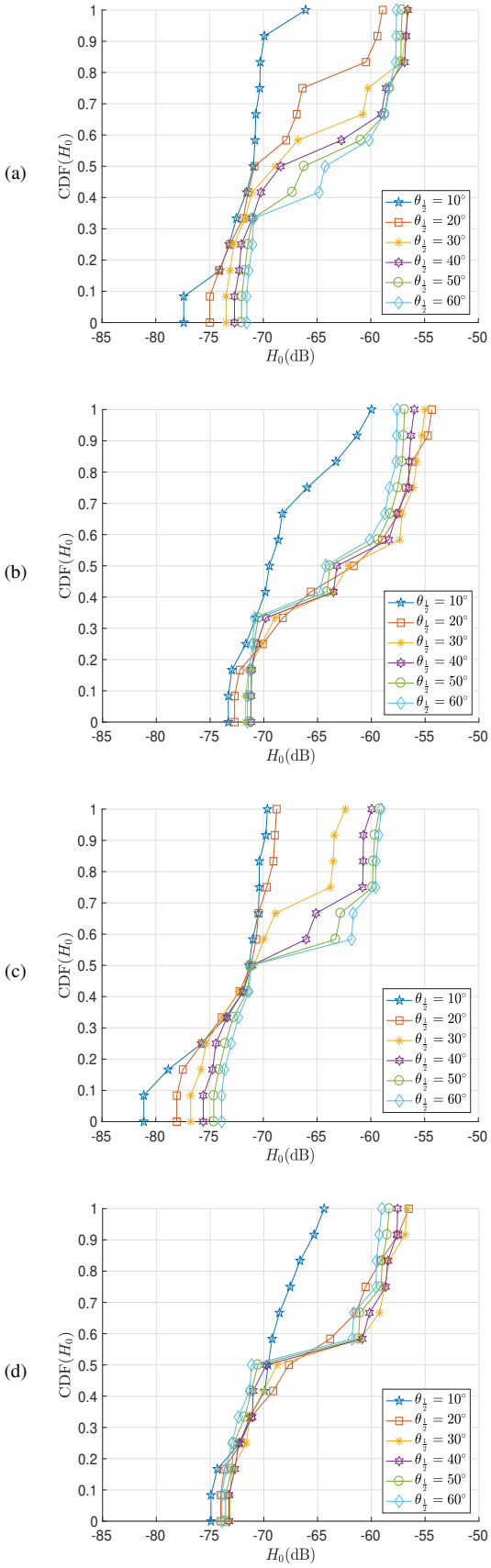

Fig. 7. Head movement: CDF of H_0 for (a) pilot uplink, (b) pilot downlink, (c) co-pilot uplink and (d) co-pilot downlink.

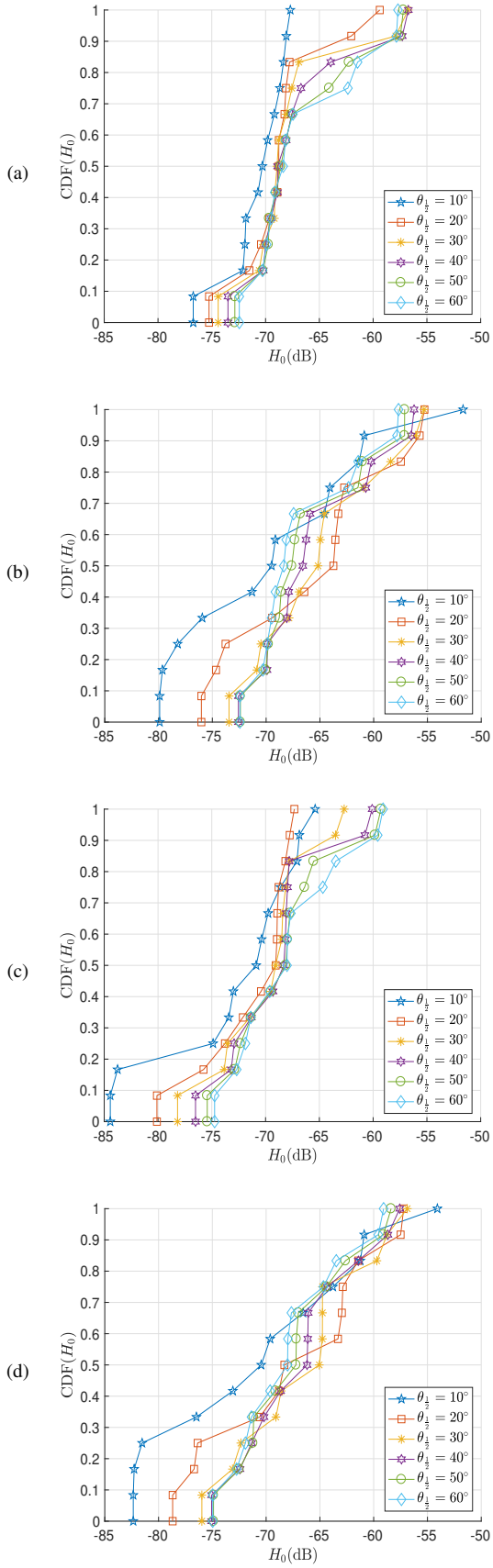

Fig. 8. Body movement: CDF of H_0 for (a) pilot uplink (b) pilot downlink, (c) co-pilot uplink and (d) co-pilot downlink.

The corresponding channel gain CDFs for pilot uplink and downlink are given in Fig.9. It can be noted that whatever the $\theta_{\frac{1}{2}}$ value, the channel gain is relatively constant when the LOS link is not blocked (about 75% of the time in the proposed scenario, in green circles), highlighting the weak impact of the moving body, regardless of the link direction. When the LOS link is obstructed (red circles), the optimal $\theta_{\frac{1}{2}}$ angle always appears to be 60° for the uplink. For the downlink, the impact of the angle value is much lower. Even if the optimal angle is 10°, the gain difference with an angle of 40° is only 0.4 dB. Thus, we can always consider an optimal value of 40° as for the scenarios 1 and 2. We can note that the obstruction of the LOS link, although due to different obstacles that are the pilots head in scenario 2 and the body of the third crew member in scenario 3, leads to almost identical minimum gains, i.e. about -72 dB. However, these results only relate to the case of a single obstructing element.

In Fig.10, we present the results obtained using the combination of dynamic scenarios 1 and 3, considering the movement of the pilot's head and the presence of the body of another crew member at the worst location in terms of blockage, shown in yellow in Fig.6. For the uplink Fig.10(a) shows similar behavior to that without a shadowing effect (cf. Fig.7(a)). Again it clearly indicates an optimal $\theta_{\frac{1}{2}}$ of 60°.

For the downlink, Fig.10(b) shows a lower impact of the angle, the gain difference between 10° (the optimal one) and 40° being only 0.89 dB, whereas it was 2.12 dB in favour of 40° for scenario 1 (cf. Fig.7(b)). So as before, an optimal angle of 40° can be retained.

Thus we can extend to this third scenario the optimal half-power angles determined for the two previous scenarios. Although they are not presented for the sake of brevity, identical results were obtained regarding the co-pilot and the combination of scenarios 2 and 3.

We conclude that the optimal values of the source half-power angles are respectively 40° on the AP side (for the downlink) and 60° on the headset side (for the uplink) regardless of the pilot and the dynamic scenario.

4) Impact of reflectivity ρ: As presented in Section II-B2, all previous results were obtained by considering an overall reflectivity ρ of 0.5, for all the materials found in the cockpit except the windscreen. Although this value is an average, often used when material properties are unknown, its potentially significant impact on the optimal half-power angle must be studied. To this end, simulations were carried out in the cockpit using different ρ values between 0.1 and 0.9, in both uplink and downlink, and for both the pilot and the co-pilot.

Fig.11 shows the CDF of H_0 values for the pilot and the two extreme values of ρ, being 0.1 and 0.9, for both uplink and downlink, using scenario 1 (head movement). The overall behavior is the same as for ρ = 0.5: the minimum gain values, corresponding to an NLOS path and being multi-reflected, are impacted by the reflectivity coefficients ρ, but the optimal $\theta_{\frac{1}{2}}$ is always 60°/40° for uplink and downlink, regardless of the ρ value.

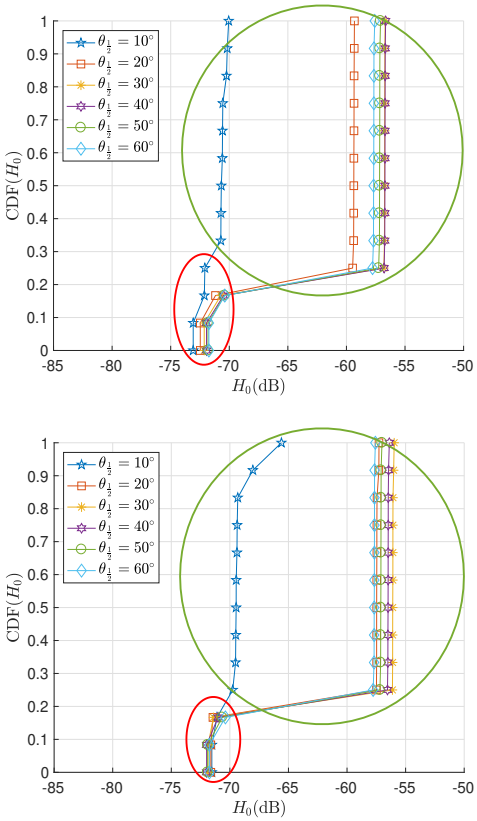

Fig. 9. Mobility scenario: CDF of H_0 for (a) pilot uplink (b) pilot downlink. Red/green circles indicate blocked/not-blocked LOS link.

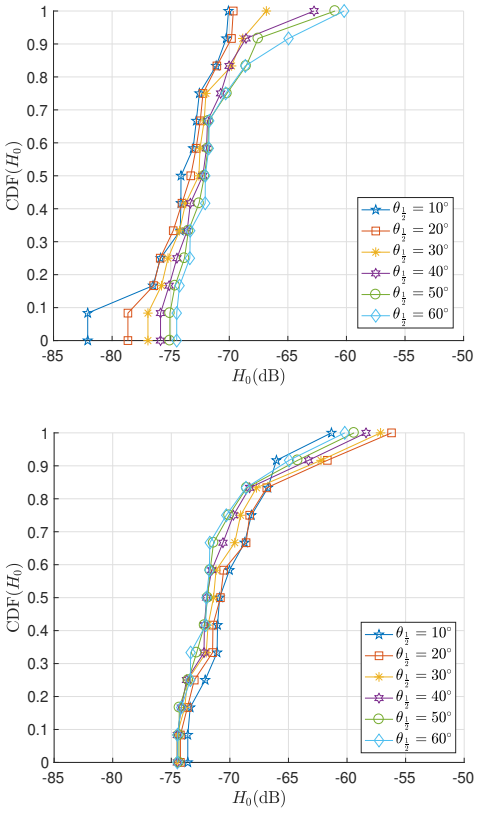

Fig. 10. Scenario 1-3: CDF of H_0 for (a) pilot uplink (b) pilot downlink.

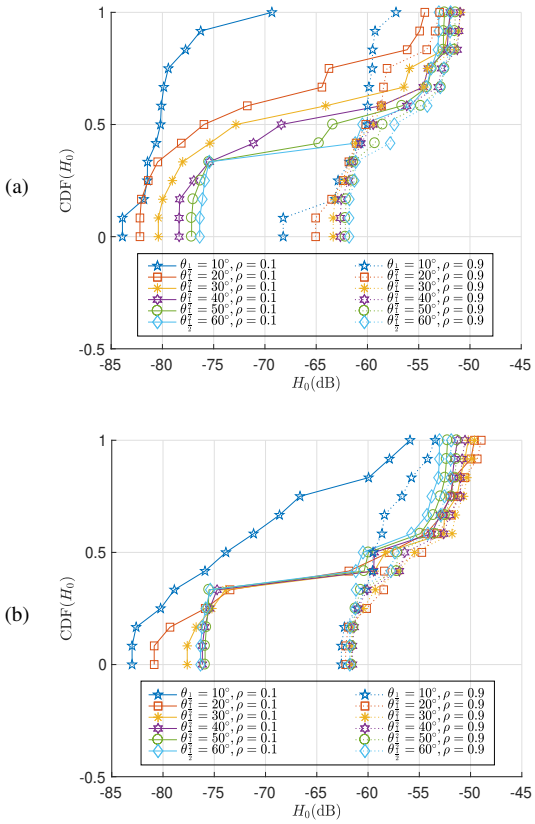

Fig. 11. Head movement: CDF of H_0 for pilot and two ρ values (a) uplink and (b) downlink.

B. Simplified model

1) Dynamic scenarios: Fig.12 reports the results of the parametric study of the half-power angle $\theta_{\frac{1}{2}}$ by considering the simplified cockpit model of Fig.1(c) and (d), with a single reflectivity value ρ equal to 0.5. For brevity, only the results for the pilot and the first two scenarios (head and body movements) are presented. Nevertheless, results for co-pilot and scenario 3, corresponding to a crew member moving inside the cockpit, led to the same conclusions.

From the analysis of these curves we deduced that the optimal pairing of $\theta_{\frac{1}{2}}$ is still 60°/40° for the uplink and the downlink respectively.

2) Impact of reflectivity ρ and BRDF: Fig.13 shows the channel gain CDFs according to the head movement of the pilot, obtained by considering the simplified cockpit model. Once again, we find that the optimal angles remain unchanged, whatever the ρ value but also the BRDF model. Indeed, let us recall that for the simplified cockpit, the windscreen is modeled as a pure diffuse surface, using a Lambertian BRDF, like all other surfaces.

C. Overall results

Whatever the dynamic scenario, the considered pilot, the geometric cockpit model and the reflectivity/BRDF of the materials, the results clearly show optimal half-power angles of 60°/40° for the optical sources in uplink and downlink respectively. These values are used in the next section.

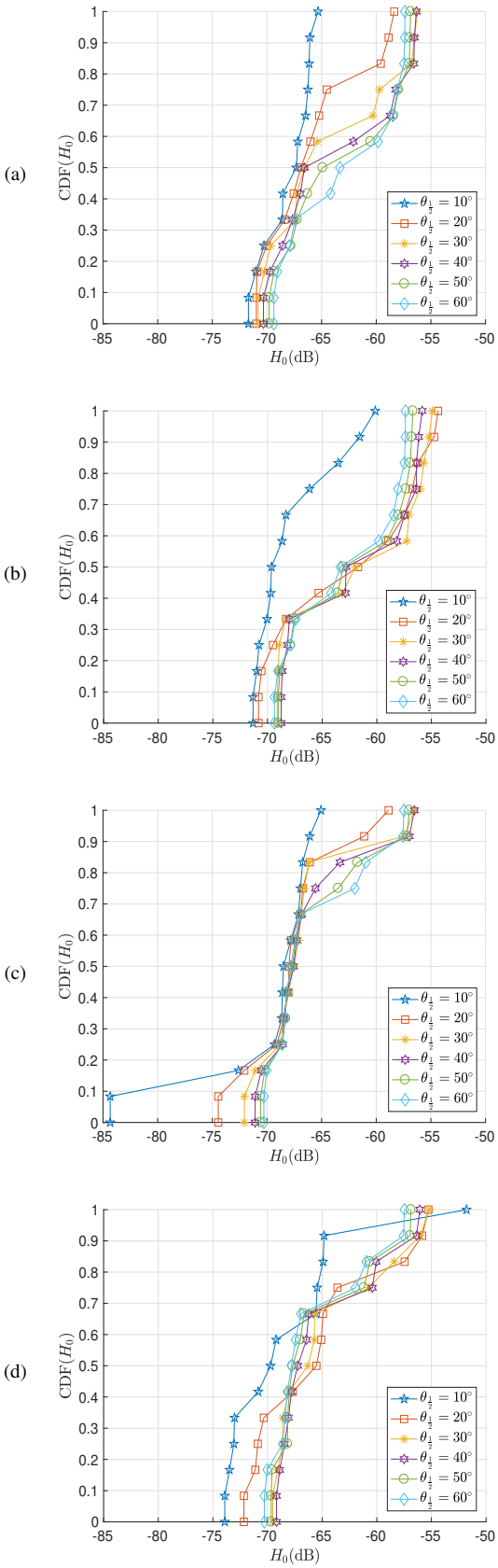

Fig. 12. Simplified cockpit: CDF of H_0 for pilot (a) head movement uplink (b) head movement downlink, (c) body movement uplink and (d) body movement downlink.

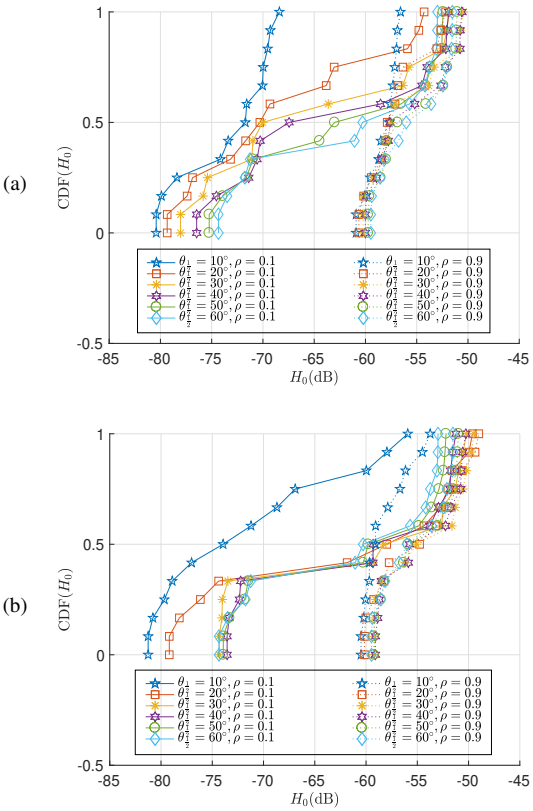

Fig. 13. Head movement and simplified model: CDF of H_0 for pilot and two ρ values (a) uplink and (b) downlink.

In addition, an important result is that a simple level of description of the environment is sufficient to determine these optimal angles. It is therefore not necessary to have a detailed model of the cockpit. Similarly, it is not necessary to set the right BRDF for the windscreen to dimension the optical sources.

In contrast, the resulting gain levels are very different depending on the geometric model, which will have an impact on the correct evaluation of performance, as shown in the following section.

IV. Performance Analysis

A. Principle

Linked to the channel gain H_0, the SNR is a classical metric used to evaluate communication channel performance, taking into account emitted power and noise. It is expressed as follows:

$$\text{SNR} = \frac{P_{R_x}^2 R^2}{\sigma^2}. \tag{8}$$

R is the photodiode responsivity set to 1 A/W in the following; P_{R_x} is the average received optical power given by:

$$P_{R_x} = P_t H_0, \tag{9}$$

where P_t is the total optical emitted power; and σ^2 represents the total noise variance assuming an additive white gaussian noise (AWGN). It is traditionally assumed that the dominant noise sources in an indoor OWC system are the background light-induced shot noise and the receiver preamplifier-induced noise [23], so that σ^2 is given by:

$$\sigma^2 = \sigma^2_{\text{shot}} + \sigma^2_{\text{therm}} \tag{10}$$

where σ^2_{shot} is the shot noise variance and σ^2_{therm} is the thermal noise variance generated by the receiver. Shot noise is generally recognized as the most limiting factor [25] so we consider here that $\sigma^2_{\text{therm}} \ll \sigma^2_{\text{shot}}$ and ignore σ^2_{therm} in the following.

Then,

$$\sigma^2 \simeq \sigma^2_{\text{shot}} = N_0 B, \tag{11}$$

where N_0 is the noise power spectral density and B is the bandwith of the modulated signal. Noise power is linked to the induced ambient photocurrent I_B by:

$$N_0 = 2qI_B, \tag{12}$$

where q is the electron quantum charge.

Finally, the SNR can be expressed as:

$$\text{SNR} = \frac{P_t^2 H_0^2 R^2}{2qI_B B}. \tag{13}$$

As it is independent of the chosen modulation, SNR is a generic criterion for characterizing the performance of a communication system. Indeed, from the distribution of gains H_0 and the bandwidth of the modulated signal B, (13) enables the prediction of the required total emitted power P_t as a function of a target SNR value. This approach can then be linked to any specific modulation, as there are theoretical and analytical formulae describing the dependency between the SNR and the bit error rate (BER), e.g. for classical OOK, where:

$$\text{BER}_{\text{OOK}} = \frac{1}{2}\text{erfc}\left(\sqrt{\frac{\text{SNR}}{2}}\right) \tag{14}$$

with erfc being the complementary error function.

Thus, to deploy the OWCs headset system in the cockpit, we propose, from any chosen modulation and according to a target BER value, i.e. a specific level of QoS, to deduce a target SNR value and finally to determine the required average optical emitted power P_t to ensure a 100% link reliability, as imposed by inflight security constraints.

B. Evaluation of ambient noise

As mentioned in the last section, the ambient noise is mainly due to the shot noise term, which itself depends on the level of the induced photocurrent I_B. For most indoor optical wireless communication systems, the main IR contributors are artificial light sources (incandescent or fluorescent) and the sun [26], [27]. The latter can even saturate the photodiode in some extreme cases where the sunlight directly falls on its FOV.

In an aircraft cockpit, the artificial illumination is weak, especially during the critical flight phases (takeoff and landing),

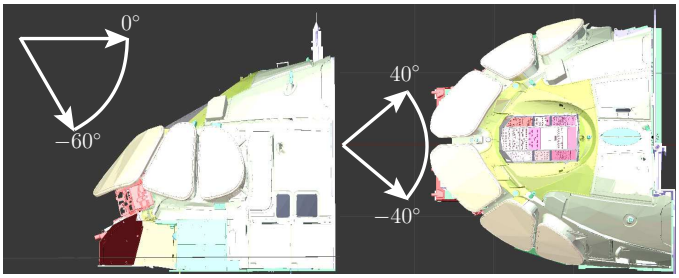

Fig. 14. Range of sun light directions of incidence onto the cockpit.

for security reasons. The crew's eyes must be accustomed to darkness in anticipation of any technical incident that could cause the airplane to fail electrically, resulting in a loss of lighting. Other potential sources of IR radiation are the display screens. For the same reason, their level of brightness is reduced. Therefore, the sun is the main source of IR radiation. There is little information in the literature regarding the level of ambient noise in the IR band for OWC applications in specific indoor environment such as aircraft cockpits. The only available information relates to values measured behind a window, in a room at ground level, as in [28], where for the IR range the typical values are 190 μA and 1000 μA depending on whether the sunshine is indirect or direct.

To assess the impact of sun noise in the cockpit, we determine the ambient photocurrent I_B from simulations of the sun contribution through the windscreen. From data on the solar spectral irradiance (for the sun at its zenith) as a function of the wavelength [29], we first deduce the contribution to the wavelength used; 940 nm. We took an average value between the data outside the atmosphere and those at sea level, which gave a level of about 0.5 W/m^2/nm. For any direction of sunlight incidence, P_A (m^2) is the area of the sunny part of the windscreen. Then, the illuminated part of the windscreen is considered as a virtual surface emitter radiating in only one direction; i.e. the sunlight direction. Finally, the contribution of this surface emitter is simulated by sampling it using the Ray-Launching based Monte-Carlo algorithm of RaPSor. Each elemental surface sample dx of the illuminated part of the windscreen radiates $0.5dx/P_A$ W/m^2. The single ray from dx in the sunlight direction either directly illuminates the receiver or reflects up to three times inside the cockpit before reaching it.

Sunlight can fall on the windscreen with very different directions of incidence depending on the season, time, location of the aircraft and its direction of flight. To take into account all the possibilities, the elevation and azimuth plans are sampled in a uniform manner, as illustrated in Fig.14.

From the elevation plane, the angle of incidence varies from 0° to -60°, whereas the azimuth angle varies from -40° to 40°. Both planes are sampled with a 20° step, which involves considering 20 directions of incidence. For each direction, and as the moving crew member does not carry a transceiver, only the first two dynamic scenarios (head and body movements) are simulated to evaluate the equivalent induced photocurrent I_B on the pilot's and co-pilot's headsets and on the AP, corresponding respectively to the downlink and uplink values

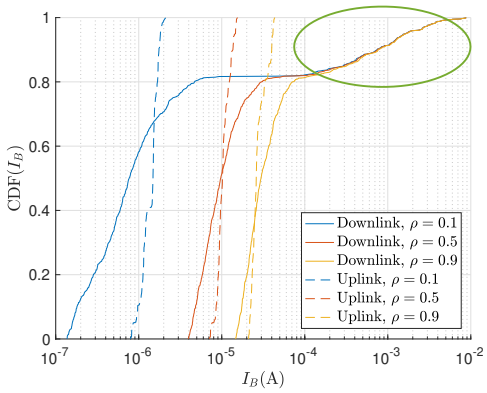

Fig. 15. CDF of I_B according to downlink/uplink and ρ.

of I_B.

The same procedure is performed according to the three considered values of ρ to evaluate the potential impact of reflected contributions. The results of scenarios 1 and 2 are concatenated to obtain the overall CDFs of I_B presented in Fig.15.

With regard to the downlink, there is a first zone of high I_B values, circled in green, which corresponds to direct sun contributions, where the induced photocurrent goes from 100 μA to 8.8 mA. For this zone, ρ has no obvious impact. The second zone of lower I_B values corresponds to indirect sun contributions. In this case the current values vary according to the ρ value. The probability of having low current values is much higher than that of having high values. To take into account a compromise between values and probability, for the rest of the article we consider an ambient noise of 774 μA corresponding to a CDF of 90%. This current value is consistent with the measurements reported in [28].

With regard to the uplink, because the AP is at the cockpit ceiling there is no direct contribution from the sun. But there is an impact from indirect contributions, which depend on the ρ value. Therefore we now consider the worst case, i.e. the 100% value of the CDF for ρ = 0.9, being I_B equal to 44 μA.

Generally windscreen manufacturers include optical filters for visible, infrared and ultraviolet wavelengths to limit the impact of the sun. However, this data is confidential. Therefore, in this article we do not take any filters into account, which can be considered a worst case scenario.

C. Impact of the environments level of description

1) Impact on H_0: The 100% link reliability objective means that communication must be guaranteed regardless of the H_0 value for pilots movements. Thus, TABLE I shows the minimum H_0 values obtained considering the two environment models presented in Section II-B1 and for different positions of the pilots and co-pilots according to the two first scenarios presented in Section II-B4 (head and body movements). From this table, we deduce the global minimum H_0 values for downlink and uplink (values highlighted in red), using a Lambertian reflectivity coefficient ρ of 0.5. These values are -75.0/-74.7 dB for the full detailed model and -69.2/-70.3 dB for the simplified one, for downlink/uplink respectively.

TABLE I
MINIMUM H_0 VALUES (dB) FOR 100% RELIABILITY, SCENARIOS 1 AND 2.

		Downlink				**Uplink**			
		Pilot		**Co-pilot**		**Pilot**		**Co-pilot**	
		Head	**Body**	**Head**	**Body**	**Head**	**Body**	**Head**	**Body**
Full detailed model	$\rho = 0.1$	-81.1	-81.4	-83.4	**-84.2**	-81.3	-81.1	**-84.0**	-83.5
	$\rho = 0.5$	-71.2	-72.6	-73.2	**-75.0**	-71.5	-72.4	-73.9	**-74.7**
	$\rho = 0.9$	-66.5	-68.2	-68.3	**-70.6**	-66.7	-68.2	-69.0	**-70.4**
Simplified model	$\rho = 0.1$	**-78.5**	-77.5	-78.4	-77.5	**-79.3**	-79.0	-79.3	-77.6
	$\rho = 0.5$	-68.8	**-69.2**	-68.5	-68.4	-69.4	**-70.3**	-69.3	-68.6
	$\rho = 0.9$	-64.1	**-65.2**	-63.6	-63.9	-64.4	**-68.0**	-64.3	-64.2

TABLE II
MINIMUM H_0 VALUES (dB) FOR 100% RELIABILITY, SCENARIOS 1 AND 2 COMBINED WITH SCENARIO 3.

		Downlink				**Uplink**			
		Pilot		**Co-pilot**		**Pilot**		**Co-pilot**	
		Sc.[1]1-3	**Sc. 2-3**	**Sc. 1-3**	**Sc. 2-3**	**Sc. 1-3**	**Sc. 2-3**	**Sc. 1-3**	**Sc. 2-3**
Full detailed model	$\rho = 0.1$	-86.3	-87.8	-89.4	**-94.2**	-84.8	-86.6	-89.6	**-95.6**
	$\rho = 0.5$	-74.6	-77.4	-77.6	**-80.6**	-74.4	-77.1	-77.8	**-81.6**
	$\rho = 0.9$	-69.2	-72.2	-72.0	**-74.6**	-69.4	-72.1	-72.3	**-75.5**
Simplified model	$\rho = 0.1$	-83.3	-85.8	-81.9	**-87.2**	-82.6	-85.8	-82.5	**-87.6**
	$\rho = 0.5$	-71.9	-73.9	-71.5	**-74.1**	-71.9	-74.0	-71.9	**-74.2**
	$\rho = 0.9$	-66.6	-68.2	-66.4	**-68.2**	-66.6	**-68.3**	-66.6	-68.2

[1] Sc. is for scenario.

The significant difference of about 5 dB in favor of the simplified model indicates that considering such a model will lead to over-estimate the channel optical gain, and so the system performance. Furthermore, these minimum H_0 values are obtained for totally different configurations according to the two considered environment models. Indeed, we find the pilot - body movement configuration for the simplified model, whereas the co-pilot - body movement is found for the full detailed model.

As presented in Section III-A3, the third scenario leads to a strong shadowing effect, when a third body is located between the AP and the headset. The corresponding minimal H_0 values obtained for the combination of scenarios 1-3 (head movement + shadowing) and scenarios 2-3 (body movement + shadowing) are presented in TABLE II. The analysis of this table firstly shows that degradation of the minimal optical gains due to shadowing implies that the worst configuration is always the combination of scenarios 2 and 3 (co-pilot body movement with third crew member shadowing). Secondly, we deduce from this table the new global minimum H_0 values for the downlink and the uplink (values highlighted in red), using a Lambertian reflectivity coefficient ρ of 0.5. These values are -80.6/-81.6 dB for the full detailed model and -74.1/-74.2 dB for the simplified one, for downlink and uplink respectively. The difference between the two environment models which was about 5 dB in favor of the simplified model for scenarios 1 and 2, shifts to about 7 dB still in favour of the simplified model when considering the shadowing effect in scenario 3. This highlights the importance of considering a detailed environment model to assess the system's performance in a realistic manner.

However, the weakest H_0 values in TABLE II, which require the combination of very specific positions of both pilot/co-pilot and the third crew member, have a very low probability of occurrence. Furthermore, the 100% reliability objective is expected only for critical flight phases, such as take-off and landing. In these specific phases, the pilot and co-pilot are alone and their movements are limited. For these reasons, the minimum channel gain values used in the next sections to assess the impact of the level of description of the environment and of the reflectivity coefficient on the system's performance, are those from TABLE I.

2) Impact on P_t: Fig.16 compares P_t as a function of the SNR for the uplink and a bandwidth B of 2 MHz, for the two cockpit models.

The overall behavior of the two curves seems similar, indicating that both models have the same relative impact. Nevertheless, there is a constant difference between the curves, corresponding to a ratio of 2.75, independent of the SNR. This means that the simplified cockpit model leads to an

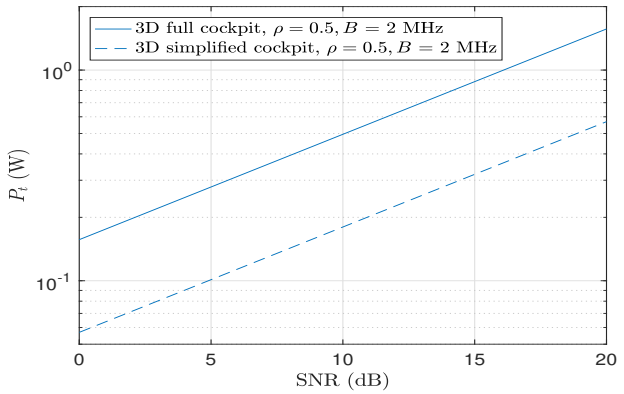

Fig. 16. P_t evolution *vs* SNR for the uplink, $\rho = 0.5$ and $B = 2$ MHz.

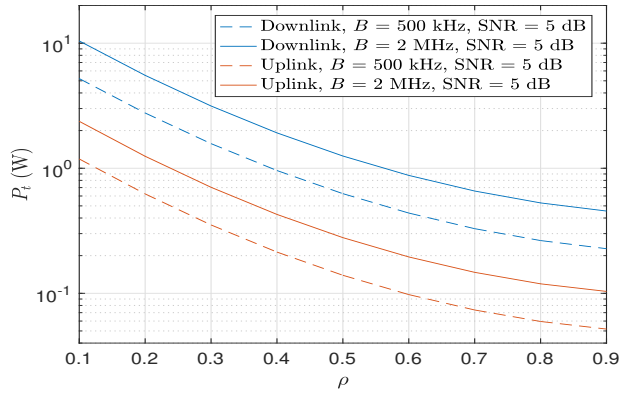

Fig. 17. P_t evolution *vs* ρ for 500 kHz / 2 MHz B and 5 dB SNR.

underestimation of the required emitted power P_t by a factor of 2.75. This corresponds to a relative error of 63.7% taking the full detailed model as a reference. In [19], the authors showed that in the case of a classical indoor environment, a detailed geometric model, including furniture, is necessary only when a high data rate is considered. The study of a complex and very confined environment, such as a cockpit, shows that a detailed model must be considered to properly assess the system's performance, even for moderate data rates.

D. Impact of reflectivity ρ

1) Full detailed model: We now focus on the ρ impact on the necessary optical power P_t. From (13) and since the evolution of ρ only impacts H_0, the results reported in Fig.17, which shows the evolution of P_t *versus* the reflectivity coefficient ρ of the cockpit, were obtained for a fixed SNR value (i.e. a fixed QoS level) of 5 dB, and two B values equal to 500 kHz and 2 MHz. In this study, the minimum H_0 values are those in red presented in TABLE I in relation to the ρ value used.

First, the global behavior was the same regardless of the link direction (down/up): obviously, the higher the reflectivity coefficient ρ, the lower the required optical P_t. Secondly and as indicated by (13), the impact of ρ was independent of the signal bandwidth B. The fact that the downlink needs more emitted power than the uplink, although the channel

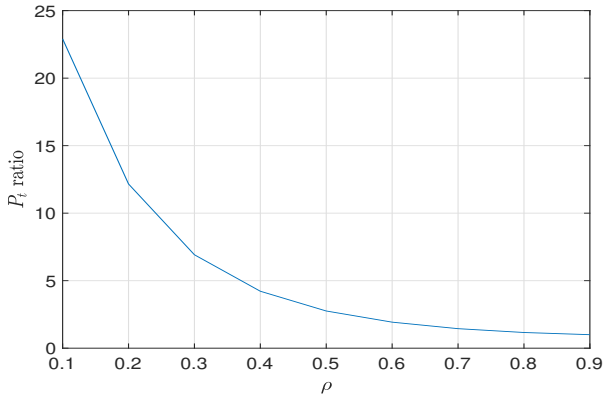

Fig. 18. Evolution of $P_t(\rho)/P_t(0.9)$ *vs* cockpit' ρ.

gains are almost the same (cf. TABLE I), is explained by the ambient noise difference, and consequently by the induced photocurrent I_B difference, as shown in Section IV-B.

Finally, Fig.18 shows the relative evolution of P_t versus ρ with regard to its value when $\rho = 0.9$, i.e. $P_t(\rho)/P_t(0.9)$, which is independent of the link direction. There was a relatively weak impact of ρ between 0.9 and 0.5, since a ratio shift ranging from 1 to 2.75 was observed. In contrast, between 0.5 and 0.1, the ρ impact increased exponentially, from a ratio of 2.75 to 22.9. This result is very interesting and generalizes those obtained in the context of the body area network [30]. It indicates the importance of establishing the reflectivity coefficients of materials in the environment under consideration, particularly for the least reflective ones, i.e. with values of ρ below 0.5. This result must also be carefully analyzed with regard to the uncertainty of the emitted irradiance for classical IR LEDs, which can vary from 2 to 5 due to differences in manufacturing processes [31], [32]. This is in the range of the error induced in P_t by an incorrect ρ, which is set between 0.5 and 0.9. For materials with ρ values in this range, it is thus not crucial to know the exact ρ of the material.

In contrast, the impact of ρ values below 0.5 is considerably higher than the error due to the emitted optical power. In this specific case it is essential to accurately know the reflectivity parameters ρ of each cockpit element in the deployment phase.

2) Simplified model: Fig.19 compares the evolution of P_t for the uplink, with (SNR, B) set to (5 dB, 2 MHz), according to the two environment models. Obviously the two curves behave similarly with ρ, but the difference between the two curves, namely the ratio of P_t for the full and simplified cockpit, depends on ρ. Indeed, it increases with a decrease in ρ. This means that the lower the reflectivity coefficient, the more the emitted power level is underestimated when using the simplified cockpit model.

To illustrate this phenomenon, Fig.20 shows the evolution of the relative error in P_t between the 3D simplified and full cockpits *versus* the reflectivity coefficient ρ, taking the full cockpit as the reference. The P_t relative error starts at 42% for ρ equal to 0.9 and then increases rapidly and stabilizes at about 67% at ρ equal to about 0.4. This error, in addition to that induced by uncertainty in ρ, shows the importance of

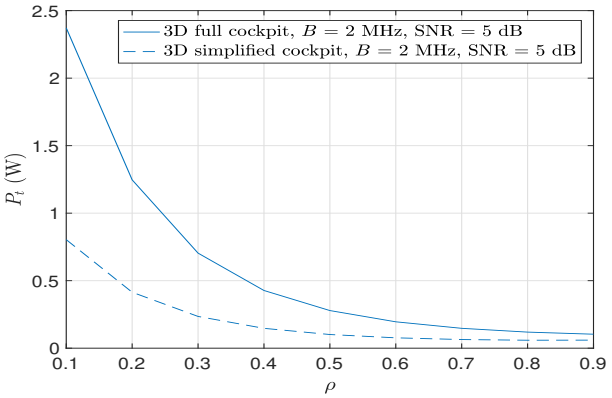

Fig. 19. P_t evolution *vs* ρ for the uplink, 2 signal bandwidths B and a 5 dB SNR.

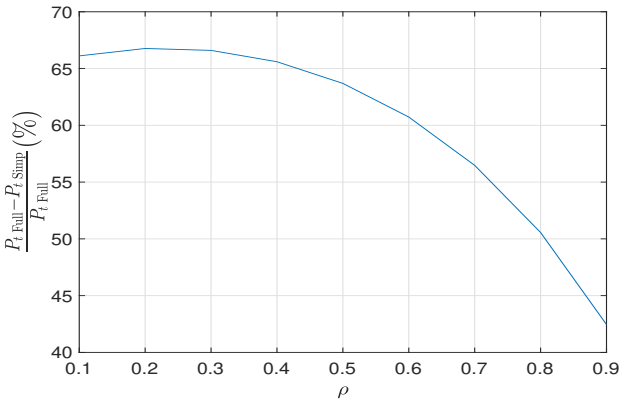

Fig. 20. Relative P_t error *vs* ρ between 3D simplified and full cockpit.

having a realistic geometric model for the dimensioning of a wireless optical link inside the cockpit.

V. Conclusion

This article has presented a study of optical wireless technology for communication between headsets worn by the crew and an AP located at the ceiling of the cockpit. The approach involved modeling the cockpit environment and the presence of the pilots using simulation software based on the ray-tracing technique associated with the Monte-Carlo method. We have integrated realistic movements of the pilot's head and body, which can affect the propagation of optical rays. In addition, we modeled the presence of another crew member moving behind the pilots, leading to blocking of the links. The studied configuration was bidirectional communication, involving only one transceiver on top of the headset and at the AP.

The overall objective of this study was to highlight the importance of each parameter involved in a simulation of light wave propagation for the determination of transceiver specifications and the communication performance. Thus, we considered the level of detail of the geometric representation of the environment, the reflectivity of the materials, and the impact of ambient noise linked to solar radiation through the windscreen.

We first studied the statistical behavior of uplink and downlink channels related to pilots movement and associated blocking effects, and to the reflectivity of the materials in the cockpit. This analysis allowed determination of the optimal values of the half-power angles of the optical sources for the uplink (60°) and the downlink (40°). We showed that a simplified model can be used to determine these optimal angles whatever the materials' reflectivity, and whatever the BRDF used for the windscreen. This is an important observation indicating that the dimensioning of such an optical wireless communication system can be achieved in other confidential environments whose data are private.

Then the performance of the system was analyzed in terms of SNR to determine the required transmitted optical power corresponding to a certain QoS have proposed the evaluation of the solar contribution through the windscreen by simulation. We demonstrated that even if a simple geometric model allows the prediction of the overall behavior of the optical wireless channel, it leads to an under-estimation of the average emission power, even for moderate data rates, unlike the results obtained for conventional indoor environments. The lower the reflectivity of the surfaces, the greater the under-estimation.

Hence, to properly assess performance we could not rely on an approximate model but need an accurate model of both geometry and materials. In this case, we showed that the impact of the reflectivity values of the cockpit's elements is quite negligible on the determination of the emission power for reflectivity values greater than 0.5. In contrast, it is very important to take into account the reflectivities for values less than 0.5 because of their higher impact on P_t. This result is a generalization of those already published, in particular in the case of body area networks.

Consequently, in future work it would be interesting to experimentally estimate the ρ values inside the cockpit in order to improve the design of the system for a given target performance level. Finally, to increase system robustness, spatial diversity could be considered not only at the headset side, as in [14], but also on the AP side. It would remove the most significant blocking effects; for example when the pilot puts his hand on top of his head and thus completely masks the transceiver from the headset.

Acknowledgment

The authors would like to thank the European Union and AIRBUS company for supporting this work through the Cleansky2 H2020 project titled Aircraft Light Communication (ALC).

References

[1] Mobile broadband: The benefits of additional spectrum. Technical report, Federal Communications Commission, Washington DC, USA, 2010.

[2] T. Cogalan and H. Haas. Why would 5G need optical wireless communications ? In *IEEE 28th Annual International Symposium on Personal, Indoor, and Mobile Radio Communications (PIMRC)*, pages 1–6, Montreal, QC, Canada, 2017.

[3] S. Arnon, J. Barry, G. Karagiannidis, R. Schober, and M. Uysal, editors. *Advanced Optical Wireless Communication Systems*. Cambridge University Press, 2012.

[4] S. Arnon, editor. *Visible Light Communication*. Cambridge University Press, 1st edition, 2015.

[5] S. Dimitrov and H. Haas, editors. *Principles of LED Light Communications Towards Networked Li-Fi*. Cambridge University Press, 1st edition, 2015.

[6] Z. Ghassemlooy, L.N. Alves, S. Zvanovec, and M-A Khalighi, editors. *Visible Light Communications: Theory and Applications*. CRC Press, 1^{st} edition, 2017.

[7] N. Schmitt. Wireless optical NLOS Communication in Aircraft Cabin for In-flight Entertainment. In *Proceedings of ESA 1^{st} Optical Wireless Onboard Communications Workshop*, 2004.

[8] S. Dimitrov, H. Haas, M. Cappitelli, and M. Olbert. On the throughput of an OFDM-based cellular optical wireless system for an aircraft cabin. In *Proceedings of the 5^{th} European Conference on Antennas and Propagation (EUCAP)*, pages 3089–3093, Roma, 2011.

[9] C. Vassilopoulos, D. Marinos, A. C. Boucouvalas, N. P. Schmitt, Th. Pistner, and C. Aidinis. Diffuse wireless optical link for aircraft intra cabin passenger communication. In *Proceedings of the 5^{th} International Symposium on Communication Systems Networks and Digital Signal Processing C.3: Optical Wireless Systems*, pages 625–628, 2006.

[10] D. Marinos, F. Leonidas, N. Vlissidis, C. Giovanis, G. Pagiatakis, C. Aidinis, C. Vassilopoulos, T. Pistner, N. Schmitt, and J. Klaue. Medical and safety monitoring system over an in-cabin optical wireless network. *International Journal of Electronics*, 98(2):223–233, 2011.

[11] S. Dimitrov, R. Mesleh, H. Haas, M. Cappitelli, M. Olbert, and E. Bassow. Path Loss Simulation of an Infrared Optical Wireless System for Aircrafts. In *GLOBECOM 2009 - 2009 IEEE Global Telecommunications Conference*, pages 1–6. IEEE, 2009.

[12] M. Kavehrad, M. I. Sakib Chowdhury, and Z. Zhou. *Short Range Optical Wireless*. John Wiley and Sons Ltd, 2015.

[13] Y. Zou, J. Zhu, X. Wang, and L. Hanzo. A survey on wireless security: Technical challenges, recent advances, and future trends. *Proceedings of the IEEE*, 104(9):1727–1765, 2016.

[14] S. Joumessi-Demeffo, P. Combeau, S. Sahuguède, B. Mercier, D. Sauveron, L. Aveneau, H. Boeglen, and A. Julien-Vergonjanne. A link reliability study of optical wireless headset inside aircraft cockpit. In *IEEE Global Lifi Congress*, Paris, France, 2019. IEEE.

[15] A. Behlouli, P. Combeau, L. Aveneau, S. Sahuguede, and A. Julien-Vergonjanne. Efficient Simulation of Optical Wireless Channel Application to WBANs with MISO Link. *Procedia Computer Science*, 40(0):190 – 197, 2014. Fourth International Conference on Selected Topics in Mobile and Wireless Networking (MoWNet2014).

[16] C. Le Bas, S. Sahuguède, A. Julien-Vergonjanne, A. Behlouli, P. Combeau, and L. Aveneau. Impact of receiver orientation and mobility on visible light communication link performance. In 4^{th} *International Workshop on Optical Wireless*, pages 1–5, Istanbul, Turkey, 2015.

[17] C. Le Bas, S. Sahuguede, A. Julien-Vergonjanne, A. Behlouli, P. Combeau, and L. Aveneau. Human body impact on mobile visible light communication link. In *IEEE Communication Systems, Networks and Digital Signal Processing*, Prague, Czech Republic, 2016. IEEE.

[18] A. Behlouli, P. Combeau, and L. Aveneau. MCMC Methods for Realistic Indoor Wireless Optical Channels Simulation. *IEEE/OSA Journal of Lightwave Technology*, 35(9):1575–1587, 2017.

[19] A. Behlouli, P. Combeau, S. Sahuguede, A. Julien-Vergonjanne, C. Le Bas, and L. Aveneau. Impact of physical and geometrical parameters on visible light communication links. In *IEEE Advances in Wireless and Optical Communications (RTUWO)*, Riga, Latvia, 2017. IEEE.

[20] Aircraft Light Communication, H2020 project funded by the European Union. https://cordis.europa.eu/project/rcn/207651/factsheet/en,https://www.facebook.com/ALCprojectH2020/.

[21] Blender. https://www.blender.org.

[22] M. Pharr, W. Jakob, and G .Humphreys. *Physically Based Rendering: From Theory to Implementation*. Morgan Kaufmann, 2016.

[23] J. M. Kahn and J. R. Barry. Wireless Infrared Communications. *Proceedings of the IEEE*, 85(2):265–298, 1997.

[24] J. R. Barry, J. M. Khan, W. J. Krause, E. A. Lee, and D. G. Messerschmitt. Simulation of multipath impulse response for indoor wireless optical channels. *IEEE Journal in Selected Areas in Communications*, 11(3):367–379, 1993.

[25] Z. Ghassemlooy, W. Popoola, and S. Rajbhandari, editors. *Optical Wireless Communications: System and Channel Modelling with MATLAB*. CRC Press, 1^{st} edition, 2012.

[26] A.C. Boucouvalas. Indoor ambient light noise and its effect on wireless optical links. *IEE Proceedings - Optoelectronics*, 143(6):334–338, 1996.

[27] S. Arnon, J. Barry, G. Karagiannidis, R. Schober, and M. Uysal, editors. *Advanced Optical Wireless Communication Systems*. Cambridge University Press, 2012.

[28] A.J.C. Moreira, R.T. Valadas, and A.M. de Oliveira Duarte. Characterisation and modelling of artificial light interference in optical wireless communication systems. In *Proc. of 6th International Symposium on Personal, Indoor and Mobile Radio Communications*, pages 326–331. IEEE, 1995.

[29] N.S. Kopeika and J. Bordogna. Background noise in optical communication systems. *Proceedings of the IEEE*, 58(10):1571–1577, 1970.

[30] T.B. Hoang, S. Sahuguede, and A. Julien-Vergonjanne. Optical Wireless Network Design for Off-Body-Sensor Based Monitoring. *Wireless Communications and Mobile Computing*, 2019:1–13, 2019.

[31] SFH 4547, OSRAM. https://media.osram.info/media/resource/hires/osram-dam-5824117/SFH+4547_EN.pdf.

[32] SFH 4775, OSRAM. https://media.osram.info/media/resource/hires/osram-dam-5667034/SFH+4775S_EN.pdf.

Pierre Combeau received the PhD degree in signal processing and telecommunications from the University of Poitiers, France, in 2004. Since 2005, he is an Associate Professor in XLIM Laboratory (UMR CNRS 7252, University of Poitiers, France). His current research includes the study of the electromagnetic waves propagation for wireless communication systems in radio and optical frequency domains.

Steve Joumessi-Demeffo received MSc degree in informatics from University of Nantes in 2016 and in Telecommunications from University of Poitiers in 2015. Since 2 years, he is a PhD candidate at the University of Limoges, France. His researches are developed within the XLIM laboratory (UMR CNRS 7252, University of Limoges, France) and concern implementation of optical wireless networks, precisely for aircraft use case.

Anne Julien-Vergonjanne received her PhD degree in Microwave and Optical Communications from the University of Limoges, France, in 1987. She is Professor since 2006 at the National School of Engineers of Limoges (ENSIL-ENSCI) and develops research activities within the XLIM laboratory (UMR CNRS 7252, University of Limoges, France). She leads the SYCOMOR research team in the SRI axis (Systems and Intelligent Networks), around optical and radio communication systems and networks. Her current research activities are in the fields of optical wireless communication systems. She is the XLIM scientific leader for European project H2020 Cleansky2 Aircraft Light Communication. She is a member of IEEE Communication Society.

Lilian Aveneau received the PhD degree in computer science, computer graphics, and light rendering from the University of Poitiers, France, in 1999. Since 2000, he is an Associate Professor in XLIM Laboratory (UMR CNRS 7252, University of Poitiers, France). His research interests include visibility between geometric objects in three-dimensional Euclidean space, rendering of shadows, global illumination, and simulation of radio and light propagation.

Stéphanie Sahuguède received her M.Sc. and M.Eng. Degrees from the National School of Engineers of Limoges (ENSIL-ENSCI), University of Limoges, France, in 2006. She received her PhD degree in high frequencies and optical telecommunications, University of Limoges, France, in 2009. She works currently as an Associate Professor in XLIM Laboratory (UMR CNRS 7252, University of Limoges, France) and ENSIL-ENSCI. Her research activities include error correction codes, optical CDMA, wireless optical communications and communication systems for e-Health.

Hervé Boeglen received the BSc, MSc and PhD degrees from the University of Haute Alsace, France in 1993, 2004 and 2008 respectively, all in Electrical Engineering. He is currently an Associate Professor at the XLIM Laboratory (UMR CNRS 7252, University of Poitiers, France). His current research interests are in the areas of digital communications, wireless channel measurement and modelling, Software Defined Radio and embedded systems for the IoT.

Damien Sauveron received his MSc and PhD degrees in Computer Science from the University of Bordeaux, France. He is Associate Professor with Habilitation at the XLIM Laboratory (UMR CNRS 7252, University of Limoges, France) since 2006. He is Head of the Computer Science Department in the Faculty of Science and Technology at the University of Limoges. Since 2011, he has been a member of the CNU 27, the National Council of Universities (for France). He has been chair of IFIP WG 11.2 Pervasive Systems Security since 2014, having previously been appointed vice-chair of the working group. His research interests are related to smart card applications and security (at hardware and software level), RFID/NFC applications and security, mobile network applications and security (particularly UAV), sensor network applications and security, Internet of Things (IoT) security, cyber-physical systems security, and security certification processes. In December 2013, the General Assembly of IFIP (International Federation for Information Processing) awarded Dr Sauveron the IFIP Silver Core award for his work. He has been involved in more than 100 research events in a range of capacities (including PC chair, General Chair, Publicity Chair, Editor/Guest Editor, Steering Committee member, and Program Committee member). He has served as external reviewer for several PhD theses in foreign countries and in France. More on http://damien.sauveron.fr/